Chapter 2

Literature Reviews

In this chapter represents 4 topics viz, thermoelectricity theorem, thermoelectric material, thermoelectric device and references.

Thermoelectricity Theorem

Thermoelectric effect

The conventional flows of heat and electricity in a material and the potentials producing them are nonreversible processes. A classic example of this fact is the production of electrical resistance heat at the rate $Q = I^2R$, regardless of the direction of flow of the electricity; although it is impossible to generate a current (I) in the conductor simplied by supplying the heat (Q) to the resistance volume R. However, there are reversible processes known as the Seebeck effect, the Peltier effect and the Thomson effect.

1. Seebeck effect

The Seebeck effect was discovered in 1823 by Thomas Johann Seebeck results in an emf in a circuit composed of two different homogeneous materials if the junctions of the materials are at different temperatures. For small temperature differences, the emf depends on the temperature difference and function of the material used. The Seebeck coefficient between the materials A and B is S_{AB}. E_{AB} and S_{AB} are positive if conventional current flows from A to B at the hot junction (Russche, 1964, pp. 4-5).

$$E_{AB} = S_{AB}\Delta T = \left(S_A - S_B\right)\Delta T \qquad (2.1)$$

Actually the Seebeck coefficient of a pair of materials is the difference of absolute coefficients.

2. Peltier effect

The Peltier effect was discovered in 1832 by Jean Charles Athanase Peltier. Whenever a circuit was composed of two dissimilar materials carries an electric current, heat is absorbed at one junction released at the other at a rate that is proportional to the current. This is called the Peltier effect, and the heat transferred is called the Peltier heat. Resistance heating is exactly nonreversible and proportional to the square of the current. The Peltier coefficient, Π_{AB}, is positive if current flow is from A to B at the junction where heat is absorbed, and the coefficient is really the difference of the absolute coefficients as in the Seebeck effect (Russche, 1964, pp. 5-6).

$$\frac{dQ_{AB}}{dt} = \Pi_{AB} I = \left(\Pi_A - \Pi_B\right) I \qquad (2.2)$$

3. Thomson effect

W. Thomson studied the Seebeck and Peltier effects, and derived a relation between their coefficients. He also predicted a new effect called the Thomson effect which is related to the reversible absorption or release of heat in a homogeneous conductor carrying a current through a temperature gradient. The rate of heat absorbed per unit length of conductor is equal to the positive coefficient times the conventional current and temperature gradient which are both in the same direction (Russche, 1964, pp. 6-8).

$$\frac{dQ_A}{dt} = \tau_A I \frac{dT}{dx} \qquad (2.3)$$

Where τ_A is the Thomson coefficient, I is the electric current and $\frac{dT}{dx}$ is the temperature gradient. Thomson postulated that the first and second laws of thermodynamics could be applied to the reversible thermoelectric processes alone, in the presence of the irreversible resistance heating and thermal conduction. The first law of thermodynamics requires that the work done by the

Seebeck effect in conducting a unit charge around the two conductors circuit must be equal to the thermal energy absorbed from the system.

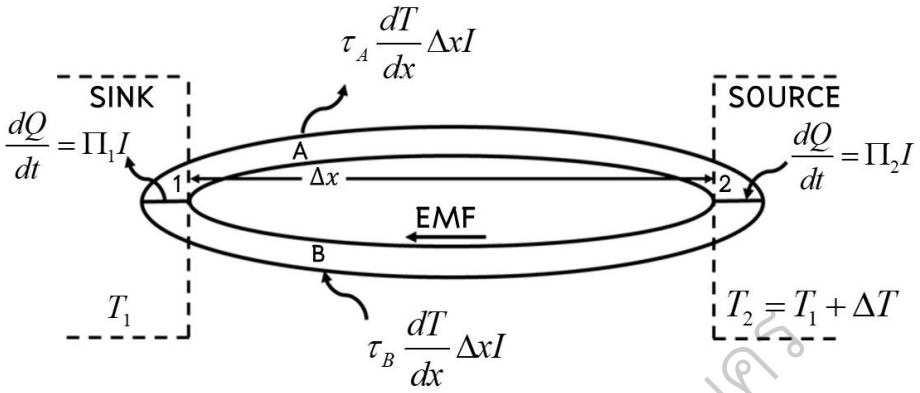

The Seebeck potential generated $EMF = S_{AB}\Delta T$

The energy required per unit charge is $E = EMF / I$

$$EMF = I\int_{T_2}^{T_1} \tau_B dT - \Pi_1 I - I\int_{T_1}^{T_2} -\tau_A dT + \Pi_2 I \tag{2.4}$$

$$E = \frac{EMF}{I} = \Pi_2 - \Pi_1 + \int_{T_2}^{T_1} (\tau_B - \tau_A) dT$$

Let $\Pi_1 - \Pi_2 = \Delta\Pi \quad \therefore \Delta E = -\Delta\Pi + (\tau_B - \tau_A)\Delta T$

The second law requires that the total change in entropy of the system due to the passage of unit charge under reversible conditions is zero.

$$0 = \frac{\Pi_1}{T_1} + \frac{\Pi_2}{T_2} + \int_{T_1}^{T_2} \frac{\tau_B - \tau_A}{T} dT \tag{2.5}$$

Differentiating equations 2.4 and 2.5 with respect to temperature gives

$$S = \frac{dE}{dT} = \frac{d\Pi}{dT} + \tau_B - \tau_A \tag{2.6}$$

$$0 = \frac{d\Pi}{dT} - \frac{\Pi}{T} + \tau_B - \tau_A \tag{2.7}$$

Subtract 2.7 from 2.6.

$$S = \frac{d\Pi}{dT} - \frac{d\Pi}{dT} + \frac{\Pi}{T}$$

$$ST = \Pi \tag{2.8}$$

Differentiating $\tau_A - \tau_B = T\frac{dS}{dT}$ $\qquad dS = (\tau_A - \tau_B)\frac{dT}{T}$

$$S_A = \int_0^T \frac{\tau_A dT}{T} \qquad d\Pi = SdT + TdS \tag{2.9}$$

$$\Pi_A = TS_A \tag{2.10}$$

These thermoelectric effects combine to provide useful power generation, heating or cooling. The efficient operation of such a thermoelectric circuit requires the optimization of the circuit and material parameters.

Thermoelectric figure of merit and the thermoelectric parameter

In 1949 the concept of a thermoelectric figure of merit, ZT, was developed by Abram Fedorovich Ioffe (Vedernikov, & Iordanishvili, 1998, pp. 37-42). The figure of merit (FOM) presented in Eq.11 describes the relationship between the three quantities determining the thermoelectric proprieties of a material: (Ohtaki., 2011, pp. 770-775)

$$ZT = \frac{\sigma S^2 T}{\kappa_{tot}} = \frac{S^2 T}{\rho \kappa_{tot}} \tag{2.11}$$

where S is the Seebeck coefficient, σ is the electrical conductivity, κ_{tot} is the total thermal conductivity, ρ is the electrical resistivity and T is the absolute temperature. In principle z is the thermoelectric figure of merit a material, however since it is temperature dependant it is more meaningful to use it in its dimensionless form ZT.

The ultimate goal is to have as high ZT as possible which implies that a good thermoelectric should possess (i) large Seebeck coefficient, in order to efficiently convert heat into electricity, (ii) high electrical conductivity to minimize ohmic losses and Joule heating due to electrical resistance and (iii) low thermal conductivity to minimize heat losses and maintain the thermal gradient (Molinari, M., Tompsett, D. A., Parker, S. C., Azough, F., & Freer, R., 2014, pp. 14109–14117). The three thermoelectric parameters are functions of the carrier concentration and are interrelated in a conflicting manner.

1. Seebeck coefficient

In an earlier section Seebeck coefficient was defined as relation between the induced voltage and the temperature difference, Eq. (1). By utilizing thermodynamics of irreversible processes, Seebeck coefficient can be expressed as (Hilaal Alama, 2012, pp. 190-212) :

$$S = \frac{8\pi^2 k_B^2}{3eh^2} m^* T \left(\frac{\pi}{3n}\right)^{\frac{3}{2}} \qquad (2.12)$$

where k_B is the Boltzman constant, e is electron charge, h is Planck's constant, m^* is the effective carrier mass, *T* is the absolute temperature and *n* is charge carrier concentration. Assuming that *S* is measured at constant temperature, the only variable in this equation will be carrier concentration *n* that can be varied through doping. By looking at the equation we can see that *S* will decrease when n increases. Reason for this is the fact that Seebeck effect is caused by the induced voltage in the material. The higher carrier concentration begins with the lower the induced voltage as it takes less new electron-hole pairs to induce current flow through the material.

2. Electrical conductivity

Electrical conductivity is obviously affected by the carrier concentration. It is derived from the Ohm law and expressed as: (Hilaal Alama, 2012, pp. 190-212)

$$\sigma = \frac{1}{R} = ne\mu \tag{2.13}$$

where μ is the carrier mobility, n is the carrier concentration and e is the electron charge.

This equation illustrates that σ increases with increasing carrier concentration and simultaneously decreasing the electrical resistivity of the material. In addition, electrical conductivity can be expressed through the Arrhenius equation: (Kabir, R., et al, 2014, 7522–7528)

$$\sigma = \frac{A}{T}\exp\left(\frac{-E_a}{k_B T}\right) \tag{2.14}$$

where A is the pre-exponential factor, k_B is Boltzmann's constant, T the absolute temperature and E_a the activation energy of conduction.

3. Thermal conductivity

In a crystalline solid, heat can be carried through the motion of charge carriers described as the electronic thermal conductivity, κ_{el}, and through the lattice vibrations, i.e. phonon thermal conductivity, κ_{ph}. As a result, the total thermal conductivity, κ_{tot} is defined as a sum of the electronic and lattice component.

$$\kappa_{tot} = \kappa_{el} + \kappa_{ph} \tag{2.15}$$

The electronic thermal conductivity can be expressed as (Bhaskar, A., Liu, C.-J., Yuan, J. J., & Chang, C.-L., 2013, pp. 236–239)

$$\kappa_{el} = L\sigma T \tag{2.16}$$

where $L = k_B^2\pi^2 / 3e^2 \sim 2.44\times10^{-8}\ \mathrm{W\Omega K^2}$ is the Lorentz number, σ is the electrical conductivity and T is the temperature.Another illustrative equation is the Wiedemann-Franz relationship *(*Fergus, J.W., 2014, pp. 525–540):

$$\frac{\kappa_{el}}{\sigma} = \left(\frac{\pi^2 k_B^2}{3e^2}\right)T \tag{2.17}$$

where e is charge of an electron and k_B is the Boltzman's constant. Both equations indicate that the ratio between σ and $\cdot\kappa_{el}$ is constant at a given temperature and any improvement in electrical conductivity leads to an offsetting increase in the electronic thermal conductivity. **The lattice thermal conductivity** dominates the heat conduction process in insulators and its contribution becomes less significant the more metallic material. Although lattice vibrations are independent of the carrier concentration, the lattice thermal conductivity increases rapidly and becomes less significant in materials with high carrier concentration because the electronic thermal conductivity is the dominating process. Lattice thermal conductivity corresponds to the propagations of phonons in the three space dimensions through the crystal lattice and can be expressed as*:* (Sootsman, Chung, & Kanatzidis, 2009, pp. 8616–8639)

$$\kappa_{ph} = \frac{1}{3}C_V v l_{ph} \tag{2.18}$$

where C_V is the heat capacity at constant volume, v is the concentration and velocity of phonons and l_{ph} is the phonon mean free path, which is defined as the average distance a phonon travels before colliding with another particle. The evolution of κ_{ph} with the temperature depends on the dominating interactions occurring in the lattice. At low temperatures those limitations are caused by the

grain size and the defect concentration while at high temperatures, collisions between phonons are the dominant factor limiting heat conduction.

Energy conversion efficiency

A thermoelectric cell is considered where the hot junction is maintained at T_2, the cold junction T_1, and power is extracted from the cell. Under steady state conditions, the temperature gradient across the cell generates a Seebeck voltage $S_{12}\Delta T$ and its resultant current I. The heat balance is stated for the hot contacts T_2. Q_a is the supplied heat to elements by the source, and Q_k that removed by conduction through the elements. Q_p is the Peltier heat removed by the current, and Q_j is the total Joule or resistance heating in the thermoelement arms. Effectively half of Q_j will appear at each junction. For a current I in the circuit, and neglecting Thomson heating (Russche, 1964, pp. 8-9) defined by Eq. 2.19.

$$
\begin{aligned}
&Q_a + \frac{1}{2}Q_j = Q_k + Q_p \\
&Q_p = \Pi_{12} I = S_{12} I T_2 \\
&Q_j = I^2\left(R_1 + R_2\right) = I^2\left(\frac{\rho_1}{D_1} + \frac{\rho_2}{D_2}\right) \\
&Q_k = \left(K_1 + K_2\right)\Delta T = \left(k_1 D_1 + k_2 D_2\right)\Delta T \\
&Q_a = S_{12} I T_2 - \frac{I^2}{2}\left(\frac{\rho_1}{D_1} + \frac{\rho_2}{D_2}\right) + \left(k_1 D_1 + k_2 D_2\right)\Delta T
\end{aligned}
\qquad (2.19)
$$

For maximum power transfer to the load, the cell resistance $R_1 + R_2$ should be equal to the load resistance R_L. Under this condition, half the voltage $S_{12}\Delta T$ appears at R_L. The useful power is thus

$$
P = \frac{\left(S_{12}\Delta T\right)^2}{4R_L} \qquad (2.20)
$$

Similarly, the optimum current I_0 occurs at maximum power transfer followed by

$$I_0 = \frac{S_{12}\Delta T}{R_L + R_1 + R_2} = \frac{S_{12}\Delta T}{2\left(R_1 + R_2\right)} \tag{2.21}$$

Then to find the cell efficiency, η, at maximum power transfer, use equation 2.20 for the useful power, and equation 2.24 evaluated at the optimum current to find the heat energy required for this output. The electrical resistivity is ρ and thermal conductivity is κ.

$$\eta = \frac{P_0}{Q_{a_0}} = \frac{\frac{S_{12}^2\Delta T^2}{4R_L}}{\frac{S_{12}^2\Delta T}{2R_L}T_2 - \frac{S_{12}^2\Delta T}{8R_L^2}R_L + \left(\kappa_1 D_1 + \kappa_2 D_2\right)\Delta T} \tag{2.22}$$

$$\eta = \frac{\Delta T}{2T_2 - \frac{\Delta T}{2} + 4\frac{\left(\kappa_1 D_1 + \kappa_2 D_2\right)}{S_{12}^2}\left(R_1 + R_2\right)} \tag{2.23}$$

$$\eta = \frac{\Delta T}{2T_2 - \frac{\Delta T}{2} + 4\frac{\left(K_1 + K_2\right)\left(R_1 + R_2\right)}{S_{12}^2}} \tag{2.24}$$

Thermoelectric materials

State of the art materials

1. Cost consideration

As mentioned in the introduction, the performance of thermoelectric materials is typically evaluated using PF, which relates directly to the device's power generation. However, when the practical application and the development of commercial devices are concerned, it is not only important to select materials which have a large value of PF, but also to include the cost of power generation-as governed by material and device manufacturing. Most of the thermoelectric devices are commercially based on the bismuth telluride (Bi-Te), lead telluride (Pb-Te), and silicon germanium (Si-Ge). Due to the high cost of tellurium and germanium, it is important to develop thermoelectric materials

which do not contain expensive elements. Furthermore, for commercialization, industries are interested in cheap materials where the price is less than copper (Cu). Therefore, the development of polymer, silicide, oxide, and other thermoelectric materials is heavily motivated by the need of lower costs and to improve the commercial viability of TEGs. The relation between raw materials and costs is shown in Figure 1 (Fitriani, 2016, pp. 635-659).

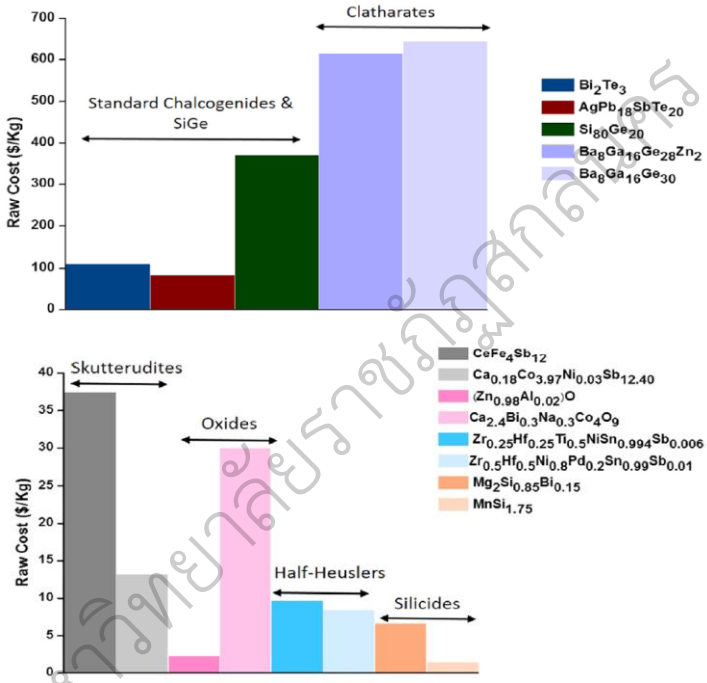

Figure 1 Cost of various thermoelectric materials based on the raw material costs of the constituent elements

2. Applicable temperature and environmental friendliness consideration

Silicides materials are promising candidates at middle temperature range between 500 and 800 K. They are very attractive as they could replace lead-based compounds due to their low cost and non-toxicity as shown in Figure 2.

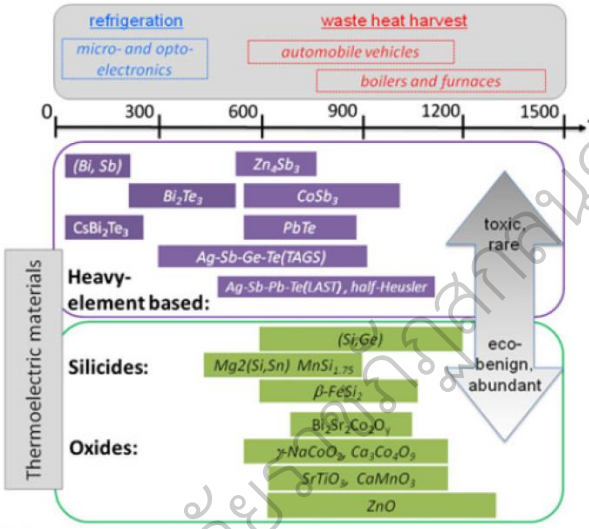

Figure 2 Schematic comparison of various thermoelectric materials in terms of the applicable temperature range, abundance and environmental friendliness (He, Liu, & Funahashi, 2011, pp. 1762–1772).

The PF of higher manganese silicide (HMS)

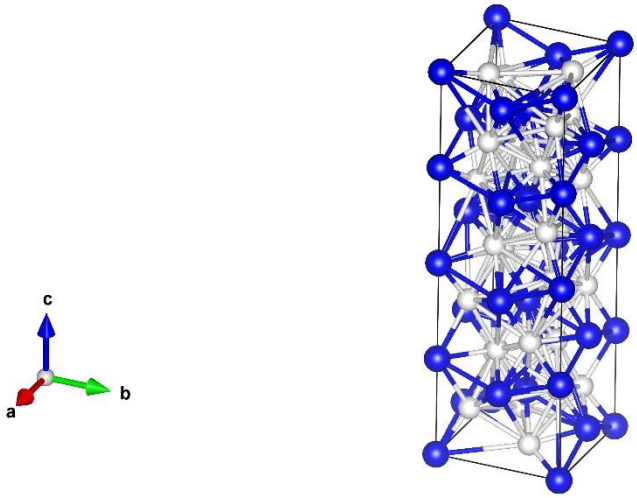

Figure 3 Crystal structure of Mn_4Si_7 (Blue ball = Mn and write ball = Si)

HMS have a tetragonal crystal structure with lattice parameter of a=5.507 Å, b=5.507 Å and c=17.390 Å as shown in Figure 3. The HMS shows the highest thermoelectric figure of merit, PF at intermediate temperatures of up to 973 K. HMS consists of a group of crystallographic structures with a chemical composition of $MnSi_{1.72-1.75}$ which includes the Mn_4Si_7, $Mn_{11}Si_{19}$, $Mn_{15}Si_{26}$ and $Mn_{27}Si_{47}$ compounds. In the past few years enhanced efforts were devoted to increase the PF values of HMS compounds.

Itoh & Yamada (Itoh & Yamada, 2009, pp. 925-929) were synthesized $MnSi_{1.73}$ by mechanical alloying and pulse discharge sintering. The sample mechanically alloyed at 400 r.p.m. for 3.6 ks gave the best thermoelectric performance. The maximum dimensionless figure of merit PF of 1.8 $mWm^{-1} K^{-2}$ was achieved at 873 K.

Luo et al (Luo, et al, 2011, pp. 404-408) were reported the PF value of $MnSi_{1.75}$ by a rapid melt-spinning process combined with a spark plasma sintering method (MS-SPS) and shows a much improved PF of 1.72 $mWm^{-1} K^{-2}$ at 700 K.

Shin, et al. (Shin, et al, 2013, pp. 1756-1761) were synthesized HMS by mechanical alloying and consolidated by hot pressing. The optimum condition of mechanical alloying was ball milling at 400 rpm for 6 h, and sound sintered compacts could be obtained by hot pressing at temperature higher than 1073 K. HMS behaved as degenerate semiconductors in that the absolute values of the Seebeck coefficient increased and the electrical conductivity slightly decreased with increasing temperature. $MnSi_{1.73}$ showed the highest PF of 0.86 $mWm^{-1} K^{-2}$ at 823 K.

Sadia, et al. (Sadia, et al, 2013, pp. 1926-1931) were reported the PF value of HMS preparing by mechanical alloying and spark plasma sintering about 1.43 $mWm^{-1} K^{-2}$ at 723 K.

Shin, et al. (Shin, et al, 2014, pp. 2104-2108) reported the PF value of Cr-doped $MnSi_{1.75}$ preparing by solid-state reaction and hot pressing. The maximum PF obtained was 1.05 $mWm^{-1} K^{-2}$ at 723 K for $MnSi_{1.73}$:$Cr_{0.01}$.

Shin, et al. (Shin, et al, 2014, pp. 1412-1415) were reported the PF value of Al-doped $MnSi_{1.73}$ preparing by solid-state reaction and hot pressing. The maximum PF was obtained as 1.35 $mWm^{-1} K^{-2}$ at 823 K for $MnSi_{1.73}$:$Al_{0.005}$.

Barczak, et al. (Barczak, et al, 2015, pp. 55–59) were reported the PF value of Fe and Al double substituted $MnSi_{1.73}$ preparing by arc-melting and annealing. The $Mn_{0.95}Fe_{0.05}Si_{1.662}Al_{0.10}$ shows a maximum PF = 1.95 $mWm^{-1} K^{-2}$ at 750 K.

Sadia, et al. (Sadia, et al, 2015, pp. 1637-1643) were reported the PF value of HMS substitution by $FeSi_2$. The maximum PF of 1.31 $mWm^{-1} K^{-2}$ at 723 K were obtained for the stoichiometric $(FeSi_2)_{0.05}(MnSi_{1.73})_{0.95}$ composition without any Si excess.

Chen, et al. (Chen, et al, 2015, pp. 30–36) were reported the PF value of HMS preparing by ball milling and spark plasma sintering. The peak PF is 1.35 $mWm^{-1} K^{-2}$ for the BM2h sample at 723 K.

Schönecker, et al. (Schönecker, et al, 2015, pp. 538 –547) were reported the progress in manufacturing higher manganese silicide material by the

ribbon-growth-on-substrate (RGS) process as show in Figure 4. The maximum PF value was found above 0.57 $mWm^{-1} K^{-2}$ at 873 K.

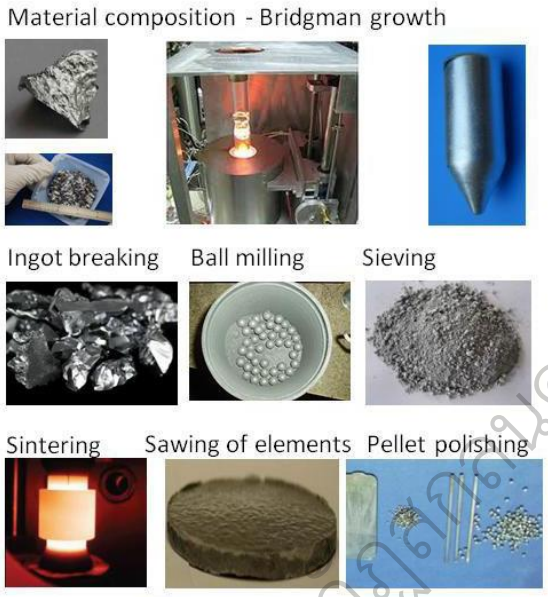

Figure 4 Show the ribbon-growth-on-substrate (RGS) process

Granger, et al. (Granger, et al, 2015, pp. 403–412) were sintered HMS from an aluminium-enriched gas-phase atomized powder using spark plasma sintering (SPS). The material exhibits the desired P-type conduction. The Seebeck coefficient has a high value for all the temperature range and in the same time the thermal conductivity is especially low. It is postulated that aluminium doping and the presence of nanometresized inclusions in the sintered microstructure are responsible for the PF around 1.82 $mWm^{-1} K^{-2}$ measured at 773 K.

Saleemi, et al. (Saleemi, et al, 2015, pp. 31–37) were fabricated nanostructured (NS) bulk $MnSi_{1.73}$ with different levels of Ytterbium inclusions via ball milling and the solid state reaction was completed by SPS. A highest PF of 1.44 $mWm^{-1} K^{-2}$ at 873 K was achieved for 1% Yb–HMS nanocomposites (NC) sample.

Truong, et al. (Truong, et al, 2015, pp. 127-132) synthesized undoped Higher Manganese Silicides, involving ball milling under soft conditions to obtain homogeneous mixtures of constituting elements, and subsequent spark plasma sintering for a direct solid state reaction. The maximum PF obtained is 1.68 $mWm^{-1} K^{-2}$ at 850 K, a high value for undoped HMS.

Sadia, et al. (Sadia, et al, 2016, pp. 71-77) synthesized HMS by arc-melting followed by hot pressing. The maximum thermoelectric figure of merit obtained is 1.13 $mWm^{-1} K^{-2}$ at 723 K, leading to ~10% PF enhancement in parallel to the pressing direction compared to the transverse direction. This shows that more carful considerations are required while assuming isotropic behavior in non-cubic polycrystalline thermoelectric materials.

Muthiah et al. (Muthiah, et al, 2016, pp. 60–64) synthesis of aluminium doped higher manganese silicides using a single-step spark plasma assisted in-situ reaction sintering process, which takes only a few minutes as opposed to few hours employing conventional processing methods. Despite employing this cost-effective material processing technique, a PF 1.46 $mWm^{-1} K^{-2}$ at 623 K was realized.

Table 1 Brief summary of PF of $MnSi_{1.75}$ base

Materials	PF ($mWm^{-1} K^{-2}$)	T (K)	Methods	References
$MnSi_{1.73}$	1.8	873	MA and pulse discharge sintering	Itoh & Yamada, 2009, pp. 925-929
$MnSi_{1.75}$	1.72	700	SPS	Luo, et al, 2011, pp. 404-408
$MnSi_{1.75}$	0.86	823	MA+HP	Shin, et al, 2013, pp. 1756-1761
$MnSi_{1.75}$	1.43	723	MA+SPS	Sadia, et al, 2013, pp. 1926-1931
$MnSi_{1.73}$:$Cr_{0.01}$	1.05	723	SSR+HP	Shin, et al, 2014, pp. 2104-2108
$MnSi_{1.73}$:$Al_{0.005}$	1.35	823	SSR+HP	Shin, et al, 2014, pp. 1412-1415
$Mn_{0.95}Fe_{0.05}Si_{1.662}Al_{0.10}$	1.95	750	AM+annealing	Barczak, et al, 2015, pp. 55–59
$(FeSi_2)_{0.05}(MnSi_{1.73})_{0.95}$	1.31	723	AM+SPS	Sadia, et al, 2015, pp. 1637-1643
$MnSi_{1.75}$	1.35	723	BM+SPS	Chen, et al, 2015, pp. 30–36
$MnSi_{1.75}$	0.57	873	RGS	Schönecker, et al, 2015, pp. 538 –547
$MnSi_{1.75}$	1.82	773	SPS	Granger, et al, 2015, pp. 403–412
1% Yb– $MnSi_{1.75}$	1.44	873	BM+SSR+SPS	Saleemi, et al, 2015, pp. 31–37
$MnSi_{1.75}$	1.68	850	BM+SPS	Truong, et al, 2015, pp. 127-132
$MnSi_{1.75}$	1.13	723	AM+HP	Sadia, et al, 2016, pp. 71-77
Al doped $MnSi_{1.75}$	1.46	623	SPAS	Muthiah, et al, 2016, pp. 60–64

The PF of Magnesium Silicide

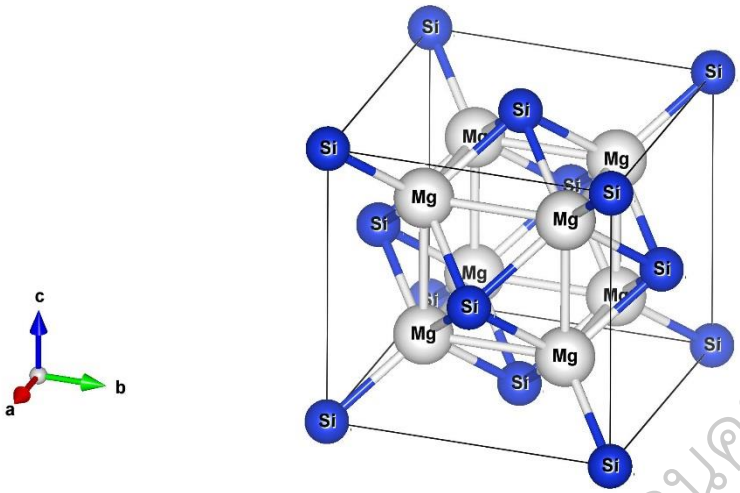

Figure 5 Crystal structure of Mg_2Si

Magnesium silicide (Mg_2Si), having a face-centered cubic CaF_2 type of structure with a=b=c= 6.36517 Å of lattice parameter as show in Figure 5. The Mg_2Si-based alloys are promising candidates for thermoelectric energy conversion for the middle high range of temperature. They are very attractive as they could replace lead-based compounds due to their low cost and non toxicity. They could also result in thermoelectric generator weight reduction (a key feature for the automotive application field). The high value of thermal conductivity of the silicide-based materials could be reduced by increasing the phonon scattering in the presence of nanosized crystalline grains without heavily interfering with the electrical conductivity of the thermoelectric material (Fiameni, et al, 2012, pp. 142–146).

Tani, & Kido (Tani, & Kido, 2005, pp. 218–224) were reported the PF value of Bi-doped Mg_2Si (Mg_2Si:Bi = 1:x) preparing by spark plasma sintering. The sample of x = 0.02 shows a maximum value of the PF is 3.49 mWm^{-1} K^{-2} at 862 K.

Song, et al (Song et al, 2007, pp. 111–117) were reported the PF value of $Mg_2Si_{1-x}Sn_x$ (x = 0, 0.2, 0.4, 0.6, 0.8, 1.0) preparing by mechanical alloying

with combination of hot pressing. A maximum PF of 0.38 $mWm^{-1} K^{-2}$ was obtained at 653K in the samples with nominal compositions of $Mg_2Si_{0.4}Sn_{0.6}$ and Mg_2Si.

Akasaka, et al. (Akasaka, et al, 2007, pp. 196–201) were reported PF value of Mg_2Si preparing by vertical Bridgman method as shown in Figure 6. The maximum PF was estimated to be 1.7 $mWm^{-1} K^{-2}$ at 656 K.

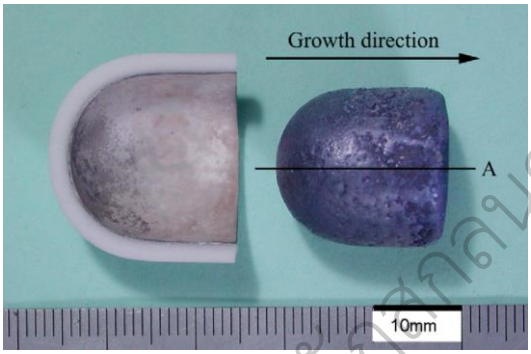

Figure 6 Ingot of Mg_2Si grown by the die-casting vertical Bridgman method

Tani, & Kido, et al (Tani, & Kido, et al, 2007, pp. 1202-1207) were reported the PF value of Sb-doped Mg_2Si (Mg_2Si:Sb = 1:x($0.001 \leq x \leq 0.02$) preparing by spark plasma sintering. The sample x = 0.005 shows a maximum value of the figure of merit PF, which is 3.48 $mWm^{-1} K^{-2}$ at 862 K.

Akasaka, et al (Akasaka et al, 2007, pp. 8237–8241) were reported the PF value of $Mg_2Si_{1-x}Ge_x$ (x=0–1.0) preparing by spark plasma sintering technique initiated from melt-grown polycrystalline $Mg_2Si_{1-x}Ge_x$ powder. The maximum PF was estimated to be 2.2 $mWm^{-1} K^{-2}$ at 750 K for samples of $Mg_2Si_{0.6}Ge_{0.4}$.

Zhang, et al (Zhang et al, 2008, pp. 9–12) were reported PF value of $Mg_{2-x}Ca_xSi$ (x = 0, 0.01, 0.03, 0.05, 0.07, 0.1) preparing by vacuum melting followed by hot pressing. The PF of Mg_2Si and $Mg_{1.99}Ca_{0.01}Si$ reach, respectively, 1.78 $mWm^{-1} K^{-2}$ at 660 K.

Tani, et al (Tani et al, 2008, pp. 335–340) were reported PF value of Al-doped $Mg_2Si_{1-x}Sn_x$ (x = 0.0–0.1) [$Mg_2Si_{1-x}Sn_x$:Al = 1:y ($0.00 \leq y \leq 0.02$)] preparing

by spark plasma sintering. Mg_2Si:Al=1:0.05 shows a maximum value of the figure of merit PF of 2.75 $mWm^{-1} K^{-2}$ at 864 K, which is 6 times larger than that of nondoped $Mg_2Si_{0.9}Sn_{0.1}$.

Luo, et al (Luo et al, 2009, pp. 96–100) were reported the PF value of $Mg_2Si_{1-x}Sn_x$ ($0 \leq x \leq 1.0$) preparing by solid state reaction and spark plasma sintering. When x = 0.2, the highest PF of 0.42 $mWm^{-1} K^{-2}$ is obtained at about 490K, which is twice as high as that of pure Mg_2Si.

You, et al (You, et al, 2011, pp. S392-S395) were reported the PF value of Bi-doped Mg_2Si (Mg_2Si:Bi_m, m = 0, 0.005, 0.01, 0.02, 0.03) preparing by solid-state synthesis and hot pressing. A maximum PF of 2.55 $mWm^{-1} K^{-2}$ was obtained for Mg_2Si:$Bi_{0.02}$ at 823 K.

Shu-cai, et al (Shu-cai et al, 2011, pp. 1785-1789) were reported the PF value of Mg_2Si preparing by solid state reaction and microwave radiation techniques. A maximum PF about 0.84 $mWm^{-1} K^{-2}$ was obtained for Mg_2Si at 600 K.

Meng, et al (Meng et al, 2011, pp. 7922– 7926) were reported the PF value of Sc- and Y-doped-Mg_2Si preparing by the field-activated and pressure-assisted synthesis (FAPAS) method. The highest PF for the Y doped (2000 ppm) samples was 2.2 $mWm^{-1} K^{-2}$ at 600 K which was higher by a factor of 1.6 than the corresponding value of pure Mg_2Si at the same temperature.

Ihou-Mouko, et al (Ihou-Mouko, et al, 2011, pp. 6503–6508) were reported the PF value of Mg_2Si:Ga_x and $Mg_2Si_{0.6}Ge_{0.4}$:Ga_x (x = 0.4% and 0.8%) preparing by direct melting in tantalum crucibles and hot pressing. The maximum value of PF was reached for the $Mg_2Si_{0.6}Ge_{0.4}$:Ga(0.8%) compound at 625K (1.03 $mWm^{-1} K^{-2}$).

Sakamoto, et al (Sakamoto, et al, 2011, pp. 8528–8531) were reported the PF value of Mg_2Si preparing by Plasma Activated Sintering technique. The maximum PF was estimated to be 2.61 $mWm^{-1} K^{-2}$ at 861 K.

Choi, et al (Choi, et al, 2011, pp. S388-S391) were reported the PF value of Bi-added Mg_2Si preparing by melting method followed by a Spark

Plasma Sintering process. The maximum value of the PF was 3.5 $mWm^{-1} K^{-2}$ with a specimen with 2 at% of Bi added at 840 K.

Fiameni, et al (Fiameni, et al, 2012, pp. 142–146) were reported the PF value of Mg_2Si:Bi=1:x for x=0.01,0.02 and 0.04 M ratio preparing by ball milling, thermal treatment and spark plasma sintering processes. The maximum PF valueof 1.65 $mWm^{-1} K^{-2}$ at 873 K was reached for the sample with x=0.02 Bi doped with the addition of Single Wall Carbon Nanohorns.

Du, et al (Du, et al, 2012, pp. 76–78) were reported the PF value of $Mg_2Si_{0.58}Sn_{0.42-x}Bi_x$ ($0 \le x \le 0.015$) preparing by hot pressing. The maximum PF is 1.54 $mWm^{-1} K^{-2}$ at 700 K for the sample x=0.015.

Hayatsu, et al (Hayatsu, et al, 2012, pp. 161–165) were reported the PF value of Sb-doped Mg_2Si preparing by Plasma Activated Sintering (PAS) technique. The incorporation of 5wt% Ni binder affected an increase in the PF value up to 3 $mWm^{-1} K^{-2}$.

Søndergaard et al (Søndergaard et al, 2012, pp. 5745–5751) were reported the PF value of $Mg_{2.2}Si_{0.3925}Sn_{0.6}Sb_{0.0075}$ and $Mg_{2.2}Si_{0.5925}Sn_{0.4}Sb_{0.0075}$ preparing by induction melting, ball milling and spark plasma sintering. The maximum PF value is up to ~2.68 $mWm^{-1} K^{-2}$ at 873 K for the $Mg_{2.2}Si_{0.5925}Sn_{0.4}Sb_{0.0075}$ compositions.

Berthebaud et al (Berthebaud et al, 2013, pp. 61–64) were reported the PF value of Mg_2Si preparing by microwave heating. The doping effect of several elements such as silver, tin, antimony, cobalt and bismuth has been studied.

n-Type and p-type Mg_2Si based materials have been successfully synthesized, with maximum PF value up to 1.8 $mWm^{-1} K^{-2}$ at 770 K.

Liu, et al (Liu, et al, 2013, pp. 352-361) were reported the PF value of $Mg_{2(1+z)}(Si_{0.3}Sn_{0.7})_{1-y}Ga_y$ preparing by . $Mg_{2.10}(Si_{0.3}Sn_{0.7})_{0.95}Ga_{0.05}$, having the optimized content of Ga and Mg, possesses the highest PF value of 1.1 $mWm^{-1} K^{-2}$ that is achieved at 650 K.

Tani, et al (Tani, et al, 2013, pp. 72-80) were reported the PF value of Mg_2Si-based composites preparing by spark plasma sintering. The maximum values of PF for the Mg_2Si composites using Bi_2O_3 was found to be 2.4 $mWm^{-1} K^{-2}$ at 865 K, respectively, which are comparable to the previously reported values of Al-, Bi-, and Sb-doped Mg_2Si.

Liu, et al (Liu, et al, 2013, pp. 333–339) were reported the PF value of $Mg_2Si_{1-x}Sn_x$-based preparing by a two-step solid state reaction followed by spark plasma sintering consolidation. This improvement come schiefly from a marginally higher Seebeck coefficient of Bi-doped solid solutions. The highest PF ~4.2 $mWm^{-1} K^{-2}$ is achieved for the y=0.03 composition at 800K.

Khan, et al (Khan, et al, 2013, pp. 606–609) were reported the PF value of Bi- and Sb-doped $Mg_2Si_{0.55}Sn_{0.4}Ge_{0.05}$ preparing by hot pressed. A high PF was obtained, with a value ~3.67 $mWm^{-1} K^{-2}$ for Bi members at 800 K.

Satyala, et al (Satyala et al 2014, pp. 141–150) were reported the PF value of Mg_2Si specimens separately doped with 2 at.% Bi and 2 at.% preparing by Mechanically alloyed and hot-pressed. A maximum PF of 2.25 $mWm^{-1} K^{-2}$, which is ~15% greater than that of the Bi-doped sample, was attained at 970 K for the sample reinforced with the conductive glass-frit.

Hu, et al (Hu, et al, 2014, pp. 485–490) were reported the PF value of Al doped Mg_2Si preparing by solid-state reaction and spark plasma sintering method. The optimal PF was 2.5 $mWm^{-1} K^{-2}$ at 844 K in the n-type Al-doped Mg_2Si material.

Ioannou et al (Ioannou et al, 2014, pp. 984–991) were reported the PF value of Bi-doped Mg_2Si preparing by solid state reaction and hot pressed method. The maximum value of the PF is found to be 2.9 $mWm^{-1} K^{-2}$ at 810 K, for $Mg_2Si_{0.97}Bi_{0.03}$.

Gao et al (Gao et al, 2014, pp. 157–162) were reported the PF value of $Mg_{2.2}Si_{1-y}Sn_{y-0.013}Sb_{0.013}$ preparing by B_2O_3 *"flux"* method followed by hot-pressing. A maximum ZT of ~1.1 at 760K was achieved for the $Mg_{2.2}Si_{0.3}Sn_{0.7-}$

$_{0.013}Sb_{0.013}$ sample arising from a high power factor of ~4×10^{-3} Wm^{-1} K^{-2} and a low lattice thermal conductivity of ~1.6Wm^{-1} K^{-1} at 760 K.

Khan et al (Khan et al, 2014, pp. 43–53) were reported the PF value of Bi-doped $Mg_2Si_{1-x-y}Sn_xGe_y$ (x = 0.4 and y = 0.05) preparing by solid state synthesis and sintering via hot pressing. The material with x = 0.02 presents the maximum value of PF about 3.2 mWm^{-1} K^{-2} at 800 K.

Zhang, et al (Zhang, et al, 2014, pp. 31–34) were reported PF value of $Mg_2(Si_{0.4-x}Sb_xSn_{0.6})$ ($0\leq x\leq 0.025$) solid solutions were prepared by an induction melting and Spark Plasma Sintering method. The PF for $Mg_2(Si_{0.38}Sb_{0.02}Sn_{0.6})$ sample shows highest value of 4.1 mWm^{-1} K^{-2} at 773 K, which is very much higher than that of the non-doped sample.

Chen, et al (Chen, et al, 2015, pp. 251–257) were reported the PF value of Mg_2Si preparing by solid-state reaction and spark plasma sintering method. The addition of 1 at.% Bi as a dopant improved the power factor significantly. Samples with 1 at.% Bi had a PF of 1.7 mWm^{-1} K^{-2} at 775 K.

Hu, et al (Hu, et al, 2015, pp. 1060-1065) were reported the PF value of $Mg_2Si_{1-x}Sn_x$ preparing by solid-state reaction and spark plasma sintering. A high PF is realized in $Al_{0.05}Mg_2Si_{0.73}Sn_{0.27}$ about 2.5 mWm^{-1} K^{-2} at 850 K, which has a notable power factor and a lower thermal conductivity.

Farahi, et al (Farahi, et al, 2015, pp. 249–255) were reported the PF value of germanium substitution for silicon in bismuth doped Mg_2Si preparing by hot pressed. The maximum PF of 1.53 mWm^{-1} K^{-2} at 773 K was obtained by $Mg_2Si_{0.677}Ge_{0.3}Bi_{0.023}$ sample.

Arai, et al (Arai, et al, 2015, pp. 45–49) were reported the PF value of Mg_2Si by Sb-doping and Ge-doping preparing by spark plasma sintering. The Ge-doped samples had a higher PF value than the PF value of the Sb-doped sample of the same concentration without Ge because the thermal conductivity of the former was lower. The maximum PF value of Sb0.23 at%-doped $Mg_2(Si_{0.995}Ge_{0.05})$ was 2.65 mWm^{-1} K^{-2} at 756 K.

Vasilevskiy, et al (Vasilevskiy, et al, 2015, pp. 523 – 531) were reported the PF value of $Mg_2Si_{1-x}Sn_x$ ($0.3 \leq x \leq 0.7$) preparing by gas atomization using a stoichiometric mixture of the commercially available high purity elements. The PF values reach a maximum of only 0.41 $mWm^{-1} K^{-2}$ at 620 K for $Mg_2Si_{0.4}Sn_{0.6}$ sample.

Du, et al (Du, et al, 2015, pp. 784-788) were reported the PF value of $Mg_{2(1+x)}Si_{0.2}Ge_{0.1}Sn_{0.7}$ ($0.06 \leq x \leq 0.12$) B_2O_3 flux method combined with spark plasma sintering technique. The electron effective mass enhancement for $x \geq 0.08$ suggests the conduction band convergence of $Mg_2Si_{0.2}Ge_{0.1}Sn_{0.7}$. $Mg_{2.16}(Si_{0.2}Ge_{0.1}Sn_{0.7})_{0.99}Sb_{0.01}$ with a maximum PF of 3.45 $mWm^{-1} K^{-2}$ at 780 K stand out as one of the best materials for intermediate temperature applications, providing a good nontoxic alternative to PbTe.

Tang, et al (Tang, et al, 2016, pp. 52–56) were reported the PF value of p-type $Mg_{2(1-x)}Li_{2x}Si_{0.4}Sn_{0.6}$ ($x = 0.00, 0.01, 0.03, 0.07, 0.09$) preparing by home-made melt spinning system combined with spark plasma sintering. Li doping dramatically reduces the thermal conductivity, leading to an enhanced PF ~1.6 $mWm^{-1} K^{-2}$ at 760 K.

Kim, et al (Kim, et al, 2016, pp. 11–15) were reported the PF value of Al and Bi co-doped Mg_2Si preparing by a solid state reaction combined with the spark plasma sintering technique. A peak PF value of 3.13 $mWm^{-1} K^{-2}$ was observed at 873 K for $Mg_{1.96}Al_{0.04}Si_{0.97}Bi_{0.03}$.

Zheng, et al (Zheng, et al, 2016, pp. 452-457) were reported the PF value of $Mg_2(Si_{0.4}Sn_{0.6})Sb_x$ ($0 \leq x \leq 0.02$) preparing by twice mechanical alloying and spark plasma sintering. The highest PF value up to 3.75 $mWm^{-1} K^{-2}$ at 673 K was obtained for $Mg_2(Si_{0.4}Sn_{0.6})Sb_{0.018}$ sample.

Table 2 Brief summary of PF of Mg_2Si base

Materials	PF ($mWm^{-1}K^{-2}$)	T (K)	Methods	References
Mg_2Si:Bi = 1:0.02	3.49	862	SPS	Tani, & Kido, 2005, pp. 218–224
$Mg_2Si_{0.4}Sn_{0.6}$	0.38	653	MA+HP	Song et al, 2007, pp. 111–117
Mg_2Si	1.7	345	Bridgman	Akasaka , et al, 2007, pp. 196–201
Mg_2Si:Sb = 1:0.005	3.48	473	SPS	Tani, et al, 2007, pp. 1202-1207
$Mg_2Si_{0.6}Ge_{0.4}$	2.2	450	SPS	Akasaka et al, 2007, pp. 8237–8241
$Mg_{1.99}Ca_{0.01}Si$	1.78	723	HP	Zhang et al, 2008, pp. 9–12
Mg_2Si:Al=1:0.05	2.75	300	SPS	Tani et al, 2008, pp. 335–340
$Mg_2Si_{0.8}Sn_{0.2}$	0.42	490	SSR+SPS	Luo et al, 2009, pp. 96–100
Mg_2Si:$Bi_{0.02}$	2.55	823	SSR+HP	You, et al, 2011, pp. S392-S395
Mg_2Si	0.84	600	SSR+MR	Shu- cai et al, 2011, pp. 1785-1789
Sc- and Y-doped-Mg_2Si	2.2	468	FA+PAS	Meng et al, 2011, pp. 7922– 7926
$Mg_2Si_{0.6}Ge_{0.4}$:Ga(0.8%)	1.03	625	Melting+HP	Mouko, et al, 2011, pp. 6503–6508
Mg_2Si	2.61	861	PAS	Sakamoto, et al, 2011, pp. 8528–8531
Bi 2% added Mg_2Si	3.5	840	Melting+SPS	Choi, et al, 2011, pp. S388-S391
Mg_2Si:Bi=1:0.02+SWCNHs	1.65	873	BM+SPS	Fiameni, et al, 2012, pp. 142–146
$Mg_2Si_{0.58}Sn_{0.405}Bi_{0.015}$	1.54	700	Melting+HP	Du, et al, 2012, pp. 76–78
Sb 1% doped Mg_2Si+ Ni 5 wt%	3	873	PAS	Hayatsu, et al, 2012, pp. 161–165
$Mg_{2.2}Si_{0.5925}Sn_{0.4}Sb_{0.0075}$	2.68	873	Melting+SPS	Søndergaard et al, 2012, pp. 5745–5751
$Mg_2Si_{0.5875}Sn_{0.4}Sb_{0.0125}$	1.8	775	SPS	Berthebaud et al, 2013, pp. 61–64
$Mg_{2.10}(Si_{0.3}Sn_{0.7})_{0.95}Ga_{0.05}$	1.1	600	SPS	Liu, et al, 2013, pp. 352-361
Sb-doped Mg_2Si	2.4	865	SPS	Tani, et al, 2013, pp. 72-80

Table 2 Brief summary of PF of Mg_2Si base (Continued)

Materials	PF ($mWm^{-1}K^{-2}$)	T (K)	Methods	References
Sb-doped Mg_2Si	2.4	865	SPS	Tani, et al, 2013, pp. 72-80
$Mg_{2.16}(Si_{0.4}Sn_{0.6})_{0.97}Bi_{0.03}$	4.2	800	SPS	Liu, et al, 2013, pp. 333–339
$Mg_2Si_{0.55}Sn_{0.4}Ge_{0.05}$:Bi=1:0.02	3.67	800	HP	Khan, et al, 2013, pp. 606–609
2%Bi doped Mg_2Si	2.25	1000	MA+HP	Satyala et al 2014, pp. 141–150
Al-doped Mg_2Si	2.5	844	SSR+SPS	Hu, et al, 2014, pp. 485–490
$Mg_2Si_{0.97}Bi_{0.03}$	2.9	810	SSR+HP	Ioannou et al, 2014, pp. 984–991
$Mg_{2.2}Si_{0.3}Sn_{0.7-0.013}Sb_{0.013}$	4	760	HP	Gao et al, 2014, pp. 157–162
Bi-doped $Mg_2Si_{1-x-y}Sn_xGe_y$	3.5	800	SSR+HP	Khan et al, 2014, pp. 43–53
$Mg_2(Si_{0.38}Sb_{0.02}Sn_{0.6})$	4.1	773	Melting+SPS	Zhang, et al, 2014, pp. 31–34
1%Bidoped Mg_2Si	1.7	775	SSR+SPS	Chen, et al, 2015, pp. 251–257
$Al_{0.05}Mg_2Si_{0.73}Sn_{0.27}$	2.5	850	SSR+SPS	Hu, et al, 2015, pp. 1060-1065
$Mg_2Si_{0.677}Ge_{0.3}Bi_{0.023}$	1.53	773	HP	Farahi, et al, 2015, pp. 249–255
$Mg_2(Si_{0.995}Ge_{0.05})$	2.65	500	SPS	Arai, et al, 2015, pp. 45–49
$Mg_2Si_{0.4}Sn_{0.6}$	0.41	620	Gas atomization	Vasilevskiy, et al, 2015, pp. 523 – 531
$Mg_{2.16}(Si_{0.2}Ge_{0.1}Sn_{0.7})_{0.99}Sb_{0.01}$	3.45	780	SPS	Du, et al, 2015, pp. 784-788
$Mg_{2(1-x)}Li_{2x}Si_{0.4}Sn_{0.6}$	1.6	760	SPS	Tang, et al, 2016, pp. 52–56
$Mg_{1.96}Al_{0.04}Si_{0.97}Bi_{0.03}$	3.13	873	SSR+SPS	Kim, et al, 2016, pp. 11–15
$Mg_2(Si_{0.4}Sn_{0.6})Sb_{0.018}$	3.75	673	MA+SPS	Zheng, et al, 2016, pp. 452-457

Thermoelectric device

Thermoelectric generators (TEGs) are devices that convert temperature differences into electrical energy, which work on the thermoelectric phenomena

known as Seebeck effect. The thermoelectric phenomena have widely been used for heating and cooling applications, however electric power generation has only been limited to niche applications e.g. thermoelectric power generators for space missions. TEG provides one of cleanest energy conversion method, which is noise-free, virtually maintenance free and can continuously produces power for several years under ambient conditions. In recent years, energy generation through thermoelectric harvesting has witnessed an increased interest for various applications, including tapping waste heat from the exhaust of vehicles, from industries, etc. The development of an efficient TEG requires the fulfillment of several factors, which includes availability of *n*- and *p*-type thermoelectric materials with high figure-of-merit (ZT), preparation of ohmic contacts between thermoelements, metallic interconnects and management of maximum heat transfer though the device (Aswal, Basu, Singh, 2016).

Skomedal, et al (Skomedal, et al, 2016, pp. 13-21) were reported power generation of thermoelectric device fabricating from *p*-$MnSi_{1.75}Ge_{0.01}$ and *n*-$Mg_2(Si_{0.4}Sn_{0.6})_{0.99}Sb_{0.01}$. The construction of the device is shown in Figure 7. The initial resistance of device at room temperature was above 8 Ω but decreased rapidly as it was heated up to higher hot side temperatures. The decreasing of resistance corresponds to the formation of a diffusion bond between the hot side electrode and the *n*- and *p*-type elements. As can be seen, resistance was reduced to a minimum value of 0.1 Ω at around 873 K. The hot side temperature was further ramped up to 1008 K were a maximum power of 3.24 W was measured under load-matching conditions and used the modeling tool COMSOL to estimate efficiencies at 1008 K and obtained values of 5.3%.

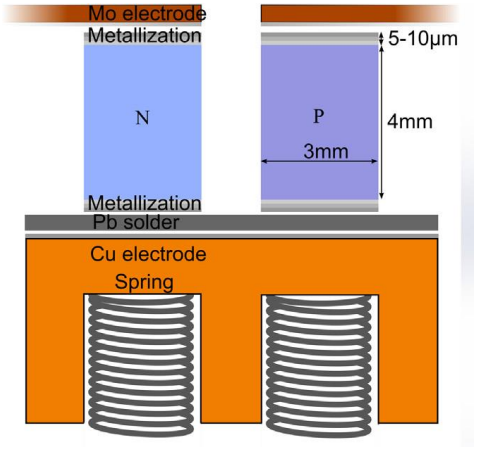

Figure 7 Sketch of unicouple with metallization and contact layers

Karina, et al (Karina, et al, 2015, pp. 588 – 595) were fabricated thermoelectric device using n-type $Mg_2(Si,Sn)$ and p-type HMS. thermoelectric samples were coated with nickel (1 μm) by sputtering. Legs for thermoelectric devices were cut from the PECS wafers, with a length of 3 mm and cross section of 5 mm × 5 mm. Devices were assembled by connecting these thermoelectric legs to an Al_2O_3 substrate with nickel-plated copper electrodes. The legs, brazing material, and substrate were arranged and then rapidly heated at 550 °C for one hour in an inert atmosphere using a homemade brazing setup. A thermoelectric device consisting of 31 pairs of thermoelectric legs is depicted in Figure 8.

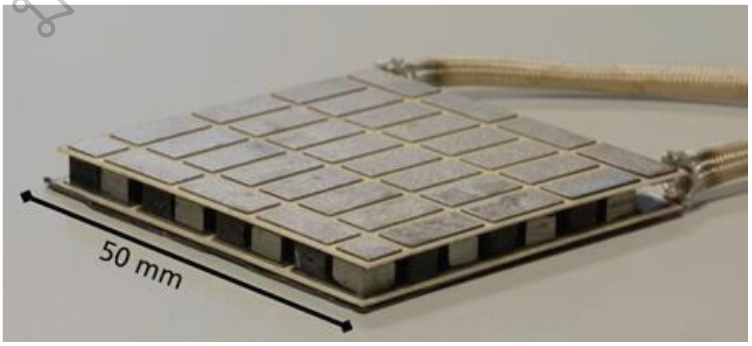

Figure 8 Thermoelectric device with 31 pairs of thermoelectric legs and a base area of 50 mm × 50 mm